Chapter 2
Theory and Simulations of SG-DBR Lasers

2-1 Analysis and Simulations of Sampled Gratings

The sampled grating shown in Fig. 2-1 is technologically simple of obtaining a reflection spectrum that has periodic maxima in the wavelength region of interest. The

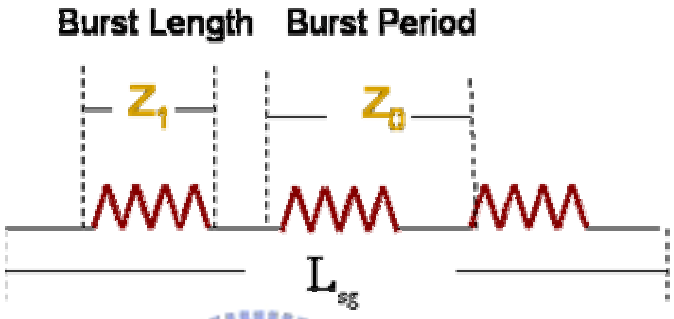

Fig. 2-1 The schematic sampled grating

sampled grating is nothing more than a conventional grating at the appropriate wavelength multiplied by a sampling function, as shown in the left column of Fig. 2-2. The reflectivity of this structure can be obtained from coupled-mode theory. The Fourier component of the sampled grating can be obtained by convolving the single Fourier component of the grating at the Bragg wavelength with the comb of Fourier components in the sampling function, as shown in right column of Fig. 2-2. The nth Fourier component $\Delta\varepsilon(n)$ in the sampled grating spectrum is related to the single Fourier component $\Delta\varepsilon_0(n)$ in the un-sampled grating spectrum by:

$$\Delta\varepsilon(n) = \Delta\varepsilon_0 \frac{Z_1}{Z_0} \frac{\sin(\frac{\pi n Z_1}{Z_0})}{\frac{\pi n Z_1}{Z_0}} \exp(\frac{i\pi n Z_1}{Z_0}) \qquad \text{(a)}$$

where

Z_1= grating burst length

Z_0=grating burst period

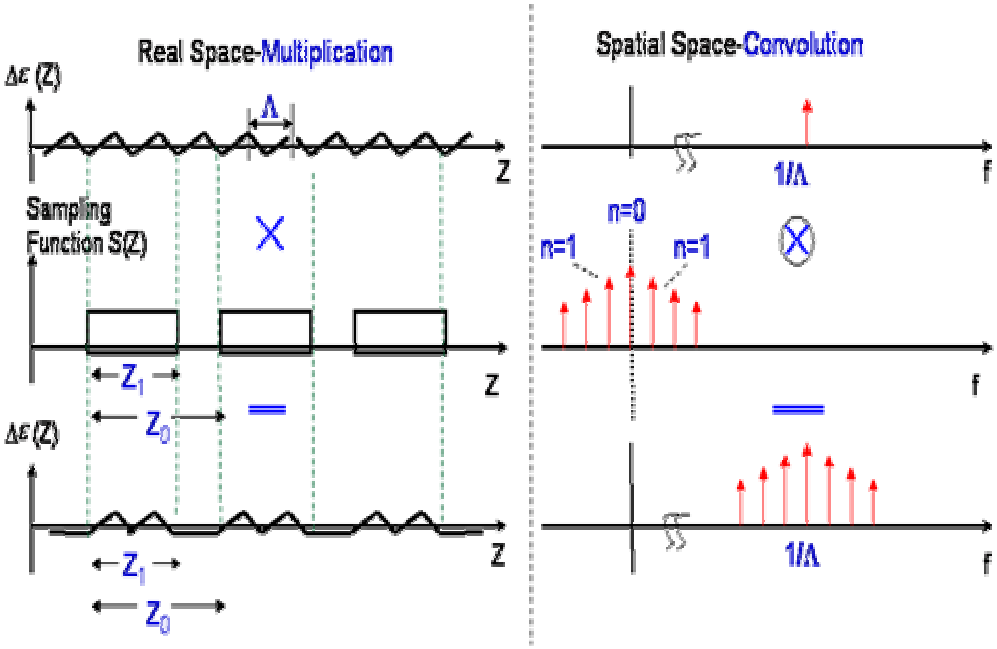

Fig. 2-2 Sampled grating and its spatial frequencies

Besides, we can invoke coupled-mode theory, which predicts that the strength of the reflection from the Fourier component n increases with the coupling strength $\kappa(n)$, which is proportional to the Fourier component. The relationship (a) between grating and sampled grating Fourier components translates directly into a relationship between grating and sampled grating coupling coefficients. If the coupling coefficient of the un-sampled grating is κ_0, then the coupling coefficient corresponding to the nth Fourier component in the sampled grating is:

$$\kappa(n) = \kappa_0 \frac{Z_1}{Z_0} \frac{\sin\left(\frac{\pi n Z_1}{Z_0}\right)}{\frac{\pi n Z_1}{Z_0}} \exp\left(\frac{i\pi n Z_1}{Z_0}\right) \qquad \text{(b)}$$

An analytic expression for reflectivity as a function of coupling coefficient is obtained by solving a pair of coupled-mode equations:

$$r(\lambda) = \sum_{n} \frac{ik^{*}(n)\sin(q(n)L_{sg})}{q(n)\cos(q(n)L_{sg}) - i\Delta\beta(n)\sin(q(n)L_{sg})} \qquad (c)$$

where

$\Delta\beta = \frac{2\pi\mu}{\lambda} + \frac{i\alpha}{2} + \frac{\pi}{\Lambda} + \frac{\pi n}{Z_0}$ = wavelength detuning from order n

$(q(n))^2 = (\Delta\beta(n))^2 - |\kappa(n)|^2$

L_{sg}= length of sampled grating

Λ = grating pitch

μ = refractive index

α =loss

The reflectivity spectrum of the sampled grating is simulated in Fig. 2-3 and a special case for the order zero is simulated in Fig. 2-4. The reflectivity spectrum of the sampled grating is comb-like with multiple equally spaced peaks which reflectivities are different. Furthermore, the spectrum also led to several observations:

1. For peak power reflectivity of order n

$$R_p(n) = \tanh^2(|\kappa(n)|L_{sg})$$

2. The spacing between reflectivity peaks is given by

$$\frac{\lambda_B^{\ 2}}{2\mu Z_0}$$

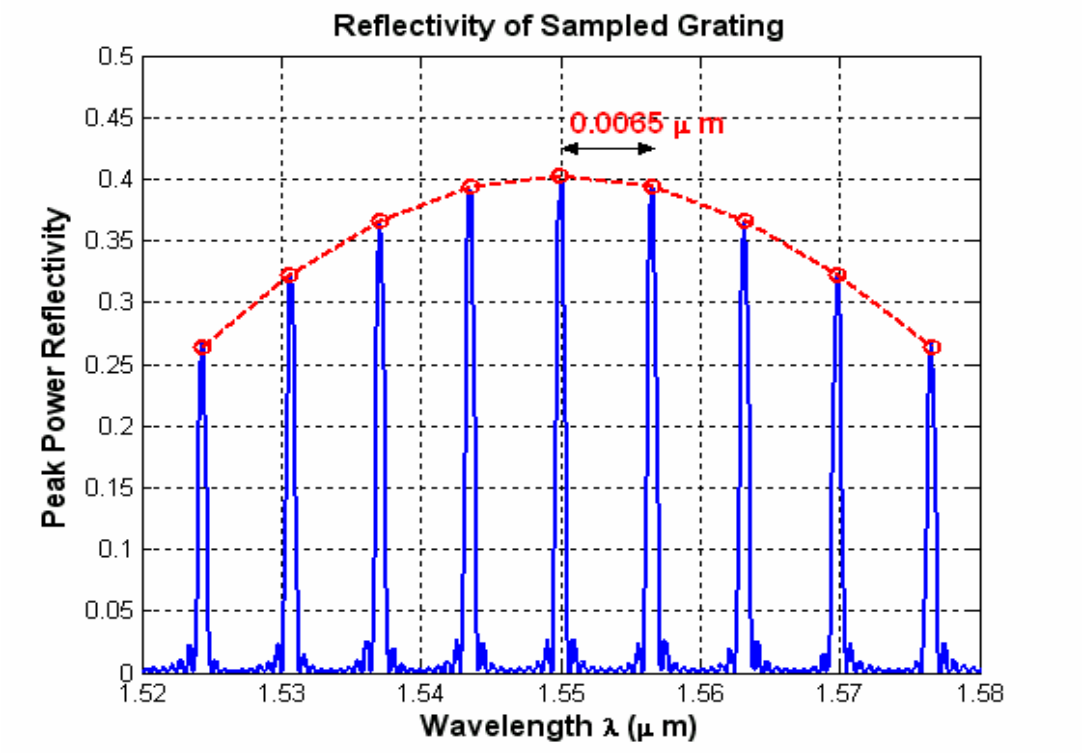

Fig. 2-3 The simulation of sampled grating reflectivity

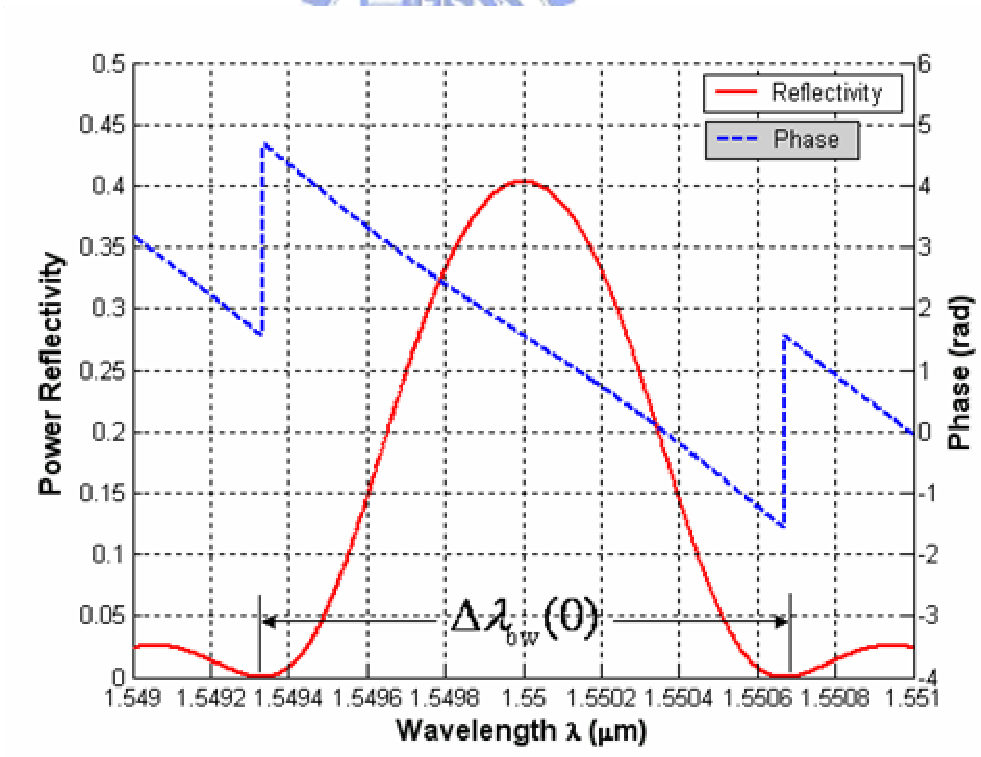

Fig. 2-4 A special case for order zero of sampled grating reflectivity

3. The envelope of reflectivity peaks widens as Z1/Z0 is reduced. Thus small duty cycle gratings are required for a large number of peaks in the spectrum. Figure 2-5 plots the number of peaks in the 3dB envelope of the reflectivity spectrum versus duty cycle. For small duty cycle, this number of peaks is approximately equal to the inverse of the duty cycle:

$$N_{3dB} \approx \mathrm{inv}(\frac{Z_1}{Z_0})$$

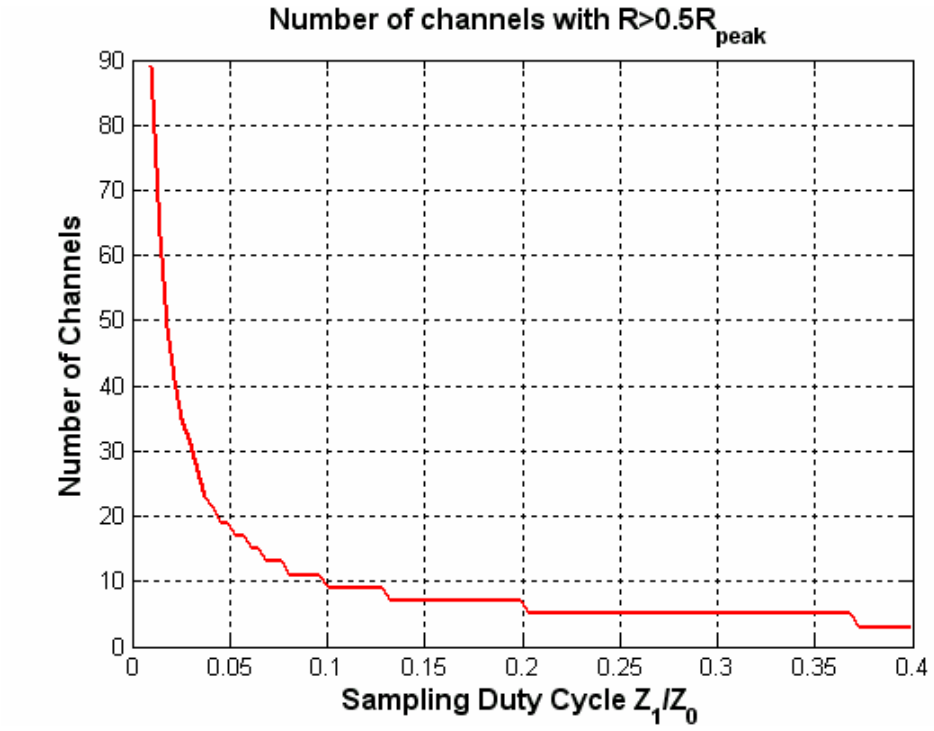

Fig. 2-5 Number of channels within 3dB envelope of sampled grating reflectivity peaks versus duty cycle.

4. The bandwidth of the peak n is given by:

$$\Delta\lambda_{bw}(n) = \frac{\lambda^2}{\pi\mu}\sqrt{|\kappa(n)|^2 + (\frac{\pi}{L_{sg}})^2}$$

For order zero in Fig. 2-4, the bandwidth is about 1.3 nm. The small effective coupling coefficient and long length of the sampled grating lead to very narrow bandwidth peaks.

2-2 Vernier Effect

The principle of Vernier is shown in Fig. 2-6. If we realize a laser structure where each end has a comb-like reflection characteristic, but where the two comb pitches are different, we can exploit the Vernier effect to expand the tuning range. The principle is illustrated in Fig. 2-7. By shifting the position of one reflectivity curve by the pitch difference $\delta\lambda$, the wavelength of coincidence shifts by $\Delta\lambda$. $\Delta\lambda$ is equal to the wavelength pitch for the other reflector.

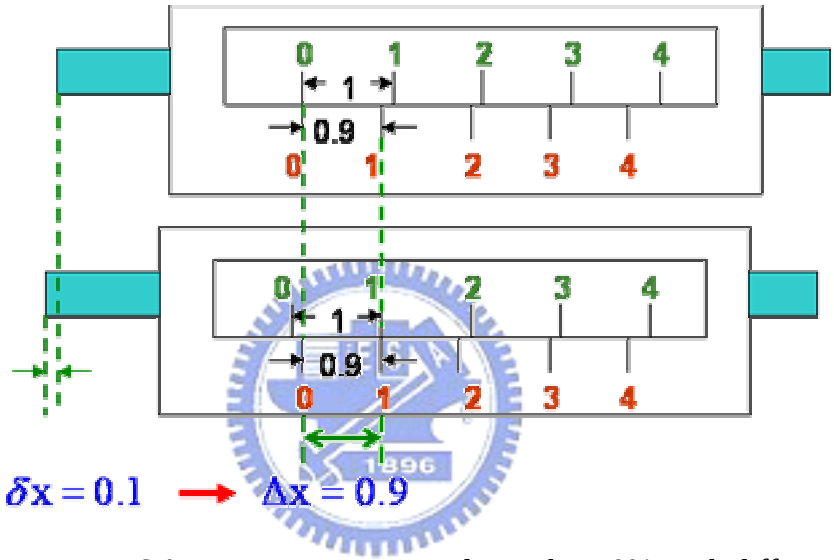

Fig. 2-6 A Vernier using two scales with a 10% pitch difference

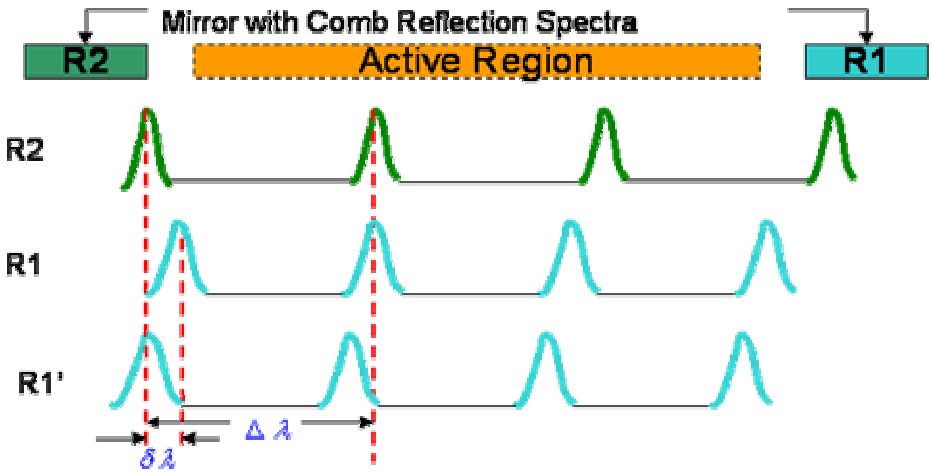

Fig. 2-7 Laser structure where each end reflectivity has a comb characteristic

2-3 Operation Principles of SG-DBR Lasers

A schematic structure of the SG-DBR laser is shown in Fig. 2-8. The SG-DBR laser consists of an active region, a phase region, a front sampled grating (SG) reflector and a back sampled grating (SG) reflector. The two SG reflectors have comb-shaped reflection spectra and slightly different peak spacing. For stable single-mode operation, peaks of each reflection comb and the longitudinal mode have to be aligned. The SG reflectors can be tuned by current injection. If one of the reflectors is tuned, different pairs of reflector peaks will successively overlap and the lasing frequency will jump by approximately the peak spacing. Medium tuning is obtained by shifting both reflectors simultaneously. The frequency will then show smaller jumps, typically about 50 or 100 GHz, corresponding to the cavity mode spacing. For fine tuning, the longitudinal modes are shifted by injecting current into the phase section. Consequently, by selecting an appropriate combination of front SG reflector, back SG reflector and phase currents, the laser can be tuned to any frequency within a range of a few THz.

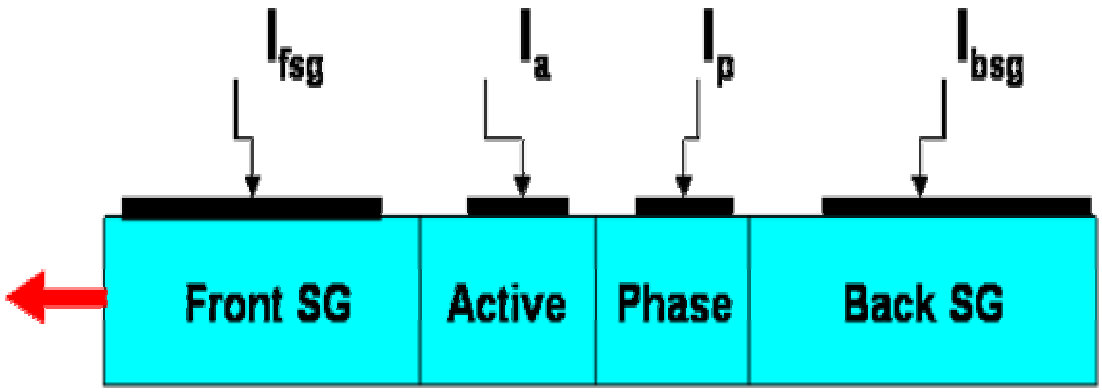

Fig. 2-8 The schematic cross-section of a SG-DBR laser

2-4 Oscillation conditions for SG-DBR lasers

In this section, we will prove oscillation conditions for the SG-DBR laser. Figure 2-9 shows a schematic structure of the SG-DBR laser. First, assume facet reflectivities are zero (r_x=0 and r_y=0). Setting a reference plane at the interface between the active and the phase sections at z=0, we write the oscillation as

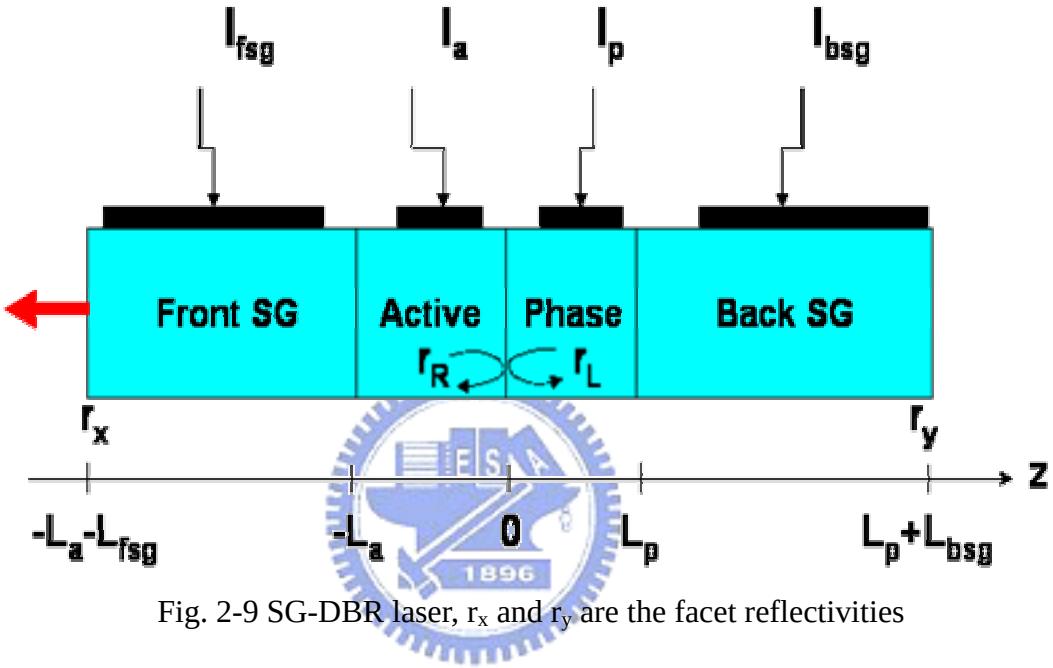

Fig. 2-9 SG-DBR laser, r_x and r_y are the facet reflectivities

$$r_L(\omega, N_a, N_{fsg}) r_R(\omega, N_p, N_{bsg}) = 1 \qquad (1)$$

where

$$r_L(\omega, N_a, N_{fsg}) = r_{fsg}(\omega, N_{fsg}) \exp(-j2k_a(\omega, N_a) L_a) \qquad (2)$$

$$r_R(\omega, N_p, N_{bsg}) = r_{bsg}(\omega, N_{bsg}) \exp(-j2k_p(\omega, N_p) L_p) \qquad (3)$$

ω = angular optical frequency

N_a= carrier density in the active section

N_p= carrier density in the phase section

N_{fsg}= carrier density in the front SG section

N_{bsg}= carrier density in the back SG section

L_a= length of the active section

L_p= length of the phase section

r_{fsg} = reflectivity of the front SG section

r_{bsg} = reflectivity of the back SG section

The complex wave numbers for the active and phase sections are given by

$$k_a(\omega, N_a) = \frac{\omega}{c}\mu_a(\omega, N_a) + j\frac{1}{2}[g(\omega, N_a) - \alpha_a(N_a)] \tag{4}$$

$$k_p(\omega, N_p) = \frac{\omega}{c}\mu_p(\omega, N_p) - j\frac{1}{2}\alpha_p(N_p) \tag{5}$$

$$= \frac{\omega}{c}[\mu_{p0} + \Delta\mu_p(N_p)] - j\frac{1}{2}[\alpha_{p0} + \Delta\alpha_p(N_p)] \tag{6}$$

from (2) and (4)

$$r_L(\omega, N_a, N_{fsg})$$

$$= r_{fsg}(\omega, N_{fsg})\exp\left\{-j2L_a\left\{\frac{\omega}{c}\mu_a(\omega, N_a) + j\frac{1}{2}[g(\omega, N_a) - \alpha_a(N_a)]\right\}\right\}$$

$$= r_{fsg}(\omega, N_{fsg})\exp[-j2L_a\frac{\omega}{c}\mu_a(\omega, N_a)]\exp\{L_a[g(\omega, N_a) - \alpha_a(N_a)]\} \tag{7}$$

from (3) and (6)

$$
\begin{aligned}
&r_R(\omega, N_p, N_{bsg}) \\
&= r_{bsg}(\omega, N_{bsg}) \exp\left\{-j2L_p\left[\frac{\omega}{c}\mu_p(\omega, N_p) - j\frac{1}{2}\alpha_p(N_p)\right]\right\} \\
&= r_{bsg}(\omega, N_{bsg}) \exp\left[-j2L_p\frac{\omega}{c}\mu_p(\omega, N_p)\right]\exp\left[-L_p\alpha_p(N_p)\right]
\end{aligned}
\tag{8}
$$

Substitute (7) and (8) into (1), we obtain

$$
\begin{cases}
\ln|r_{fsg}||r_{bsg}| + L_a(g-\alpha_a) - L_p\alpha_p = 0 \\
\exp\left[-j\left(2L_a\frac{\omega\mu_a}{c} + 2L_p\frac{\omega\mu_p}{c}\right)\right]\exp\left\{j\left[\mathrm{Arg}(r_{fsg}) + \mathrm{Arg}(r_{bsg})\right]\right\} = 1
\end{cases}
$$

$$
\Rightarrow
\begin{cases}
g = \alpha_a + \frac{L_p}{L_a}\alpha_p + \frac{1}{L_a}\ln\frac{1}{|r_{fsg}||r_{bsg}|} \\
2L_a\frac{\omega\mu_a}{c} + 2L_p\frac{\omega\mu_p}{c} - \mathrm{Arg}(r_{fsg}) - \mathrm{Arg}(r_{bsg}) = 2m\pi
\end{cases}
$$

$$
\Rightarrow
\begin{cases}
g = \alpha_a + \frac{L_p}{L_a}\alpha_p + \frac{1}{L_a}\ln\frac{1}{|r_{fsg}||r_{bsg}|} \\
2\beta_a L_a + 2\beta_p L_p - \mathrm{Arg}(r_{fsg}) - \mathrm{Arg}(r_{bsg}) = 2m\pi
\end{cases}
$$

where

β_a =propagation constant in the active section

β_p =propagation constant in the phase section

we finish proving the oscillation condition for the SG-DBR laser.

2-5 Simulations of SG-DBR lasers

We use the parameters of simulations shown in Table 2-1.

Parameter	Symbol	Value
Length of SG-DBR section	$L_{fsg} = L_{bsg}$	1000 μm
Width of waveguide layers	$W_{fsg} = W_{bsg}$	1.2 μm
Thickness of waveguide layers	$D_{fsg} = D_{bsg}$	0.23 μm
Index derivative wrt carrier density	dn/dN	$-5.97*10^{-27}$ m^3
Absorption derivative wrt carrier density	dα /dN	$2.56*10^{-21}$ m^2
Bragg wavelength without current injection	λ_B	1.55 μm
Nonradiative recombination coefficient	A	$1*10^8$/s
Radiative recombination coefficient	B	$8*10^{-17}m^3$/s
Auger recombination coefficient	C	$4*10^{-41}$ m^6/s
Loss in passive section	$\alpha_{p0} = \alpha_{fsg0} = \alpha_{bsg0}$	10/cm
Loss in active section	α_a	20/cm
Coupling coefficient of the unsampled grating	κ_0	250/cm
Grating burst length	Z1	10 μm
Front grating burst period Back grating burst period	Z_{0fsg} Z_{0bsg}	198 μm 200 μm
Equivalent refractive index	$\mu_{p0} = \mu_{fsg0} = \mu_{bsg0}$	3.6875
Grating pitch	Λ	$\frac{\lambda_B}{2\mu_{fsg}(\mu_{bsg})}$
Length of active section	La	450 μm
Length of phase section	Lp	200 μm
Confinement factor	$\Gamma_{fsg} = \Gamma_{bsg}$	0.3

Table 2-1 Parameters of simulations

2-5-1 How to Design Front and Back Sampled Reflectors?

The simulation of front SG reflector and back SG reflector spectra are plotted in Fig. 2-10. By using different burst period, peaking spacings are slightly different.

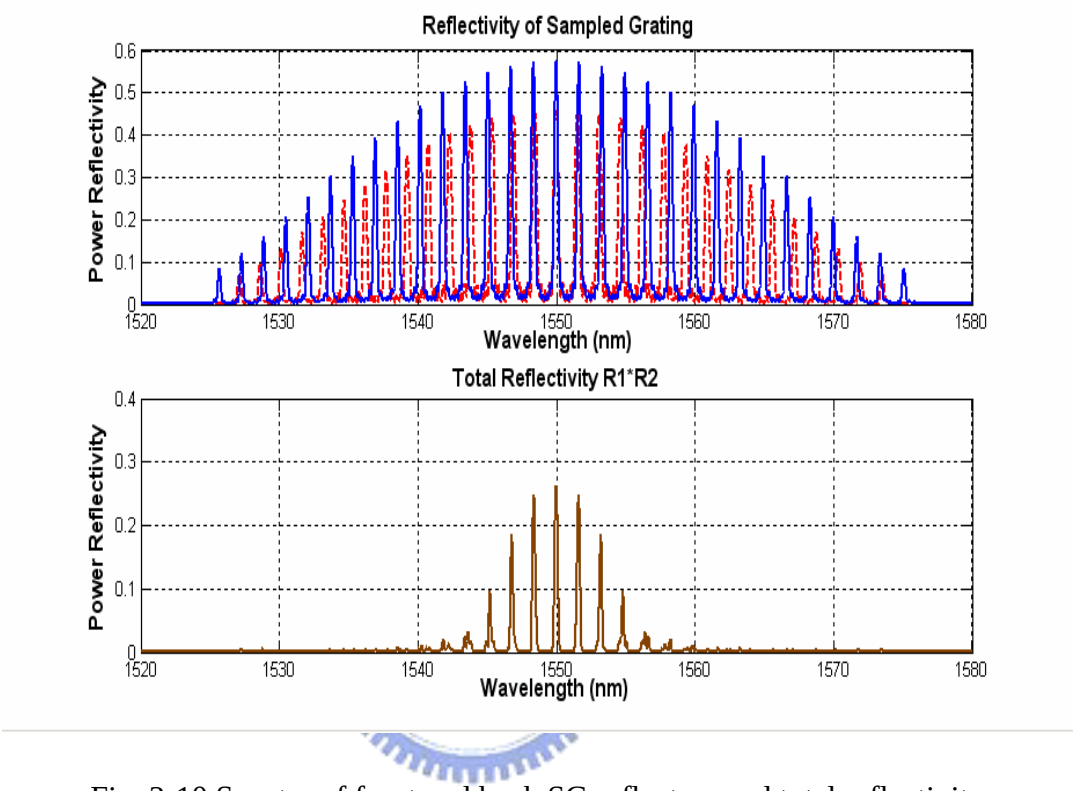

Fig. 2-10 Spectra of front and back SG reflectors and total reflectivity

2-5-2 Characteristics in Wavelength Tuning for SG-DBR Lasers

From section 2-4, the oscillation condition for the SG-DBR laser is express as

$$g = \alpha_a + \frac{L_p}{L_a}\alpha_p + \frac{1}{L_a}\ln\frac{1}{|r_{fsg}||r_{bsg}|}$$

$$2\beta_a L_a + 2\beta_p L_p - \arg(r_{fsg}) - \arg(r_{bsg}) = 2m\pi$$

The first equation denotes the gain condition, and the second denotes the phase matching condition. When current is injected into the passive section, such as the phase section or the SG section, the changes in refractive index $\Delta\mu$ and internal absorption $\Delta\alpha$ are given by

$$\Delta\mu_{fsg} = \Gamma\frac{dn}{dN}N_{fsg},\quad \Delta\mu_{bsg} = \Gamma\frac{dn}{dN}N_{bsg},\quad \Delta\mu_{p} = \Gamma\frac{dn}{dN}N_{p}$$
$$\Delta\alpha_{fsg} = \Gamma\frac{dn}{d\alpha}N_{fsg},\quad \Delta\alpha_{bsg} = \Gamma\frac{dn}{d\alpha}N_{bsg},\quad \Delta\alpha_{p} = \Gamma\frac{dn}{d\alpha}N_{p}$$

where

Γ = confinement factor in the passive section

$\frac{dn}{dN}$ = index derivative with respect to carrier density

$\frac{d\alpha}{dN}$ = absorption derivative with respect to carrier density

N_p= carrier density in the phase section

N_{fsg}= carrier density in the front SG section

N_{bsg}= carrier density in the back SG section

The carrier densities N_p, N_{fsg}, and N_{bsg} are determined by the injection currents into phase, front, and back SG sections, respectively.

$$I_p = eV_p(AN_p + BN_p^2 + CN_p^3) \quad \Rightarrow CN_p^3 + BN_p^2 + AN_p - \frac{I_p}{eV_p} = 0$$
$$I_{fsg} = eV_{fsg}(AN_{fsg} + BN_{fsg}^2 + CN_{fsg}^3) \quad \Rightarrow CN_{fsg}^3 + BN_{fsg}^2 + AN_{fsg} - \frac{I_{fsg}}{eV_{fsg}} = 0$$
$$I_{bsg} = eV_{bsg}(AN_{bsg} + BN_{bsg}^2 + CN_{bsg}^3) \quad \Rightarrow CN_{bsg}^3 + BN_{bsg}^2 + AN_{bsg} - \frac{I_{bsg}}{eV_{bsg}} = 0$$

where

e= electron charge

V_p= volume of the waveguide in the phase section

V_{fsg}= volume of the waveguide in the front SG section

V_{bsg}= volume of the waveguide in the back SG section

A= linear nonradiative recombination rate

B= radiative recombination coefficient

C= Auger recombination coefficient

The wavelength detuning for front and back SG sections is expressed as

$$\Delta\beta_{fsg}(n) = \frac{2\pi(\mu_{fsg0} + \Delta\mu_{fsg})}{\lambda} + \frac{i(\alpha_{fsg0} + \Delta\alpha_{fsg})}{2} - \frac{\pi}{\Lambda} - \frac{\pi n}{Z_{fsg0}}$$

$$\Delta\beta_{bsg}(n) = \frac{2\pi(\mu_{bsg0} + \Delta\mu_{bsg})}{\lambda} + \frac{i(\alpha_{bsg0} + \Delta\alpha_{bsg})}{2} - \frac{\pi}{\Lambda} - \frac{\pi n}{Z_{bsg0}}$$

where

μ_{fsg0} = refractive index of the front SG section without current injection

μ_{fsg0} = refractive index of the back SG section without current injection

α_{fsg0} = loss in the front SG section

α_{bsg0} = loss in the back SG section

Z_{fsg0} = grating period of the front SG

Z_{bsg0} = grating period of the back SG

Λ = grating pitch

Without injection into the passive sections, the simulations of front SG reflector and back SG reflector spectra, total reflectivity of two SG reflectors, and threshold gain are plotted in Fig. 2-11. We find the peaks alignment of two SG reflectors is at Bragg wavelength. Therefore the total reflectivity has a maximum at Bragg wavelength. As a result of a maximum of the total reflectivity at Bragg wavelength, the threshold gain has a minimum at Bragg wavelength which is the lasing wavelength.

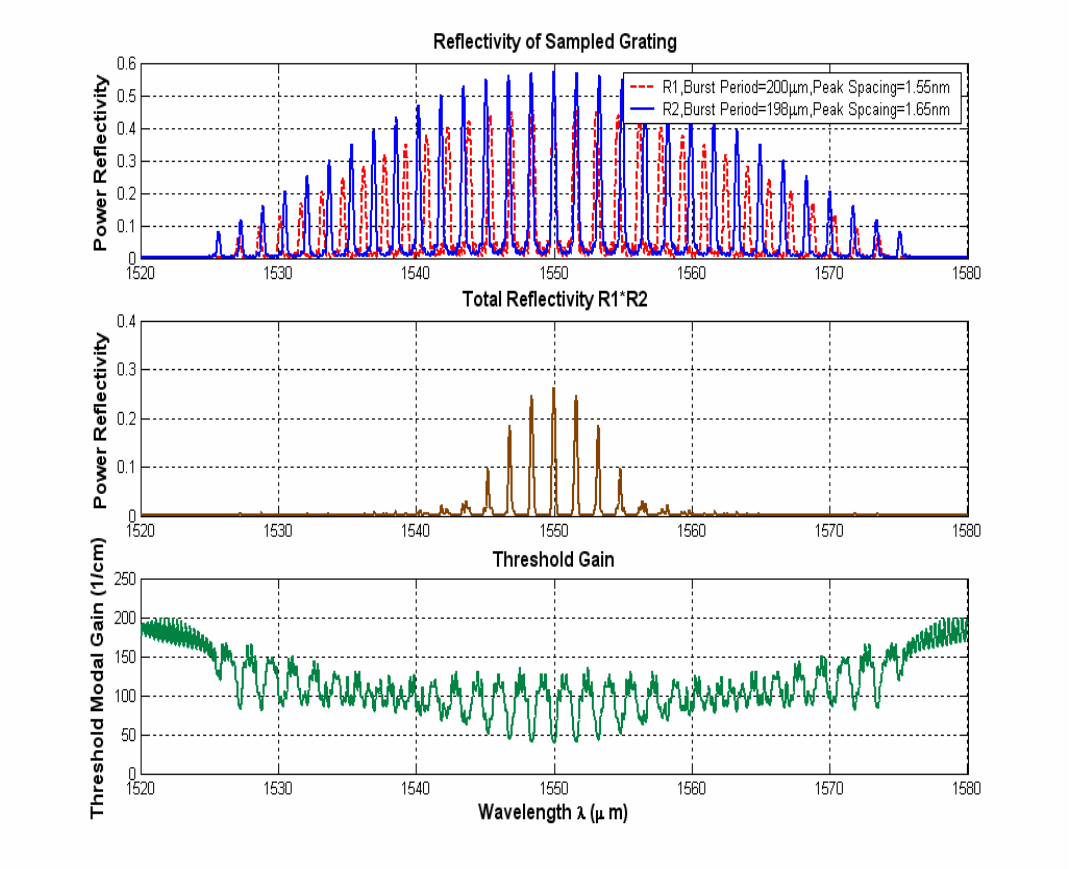

Fig. 2-11 Spectra of front and back SG reflectors, total reflectivity and threshold gain without current injection into the passive sections

When the current injected into the SG section, the Bragg frequency ω_B is taken to a linear function of carrier density N_{fsg} or N_{bsg}:

$$\omega_B = \omega_{B0} - \Gamma \frac{\omega_{B0}}{\mu_{sg}} \frac{dn}{dN} N_{sg}$$

where

ω_{B0} = Bragg frequency without carrier injection.

The calculation of Bragg frequency under different current injections is shown in Fig. 2-12. We realize that when grating current increases, Bragg frequency ω_B increases as a result of the increase of carrier density N_{sg}.

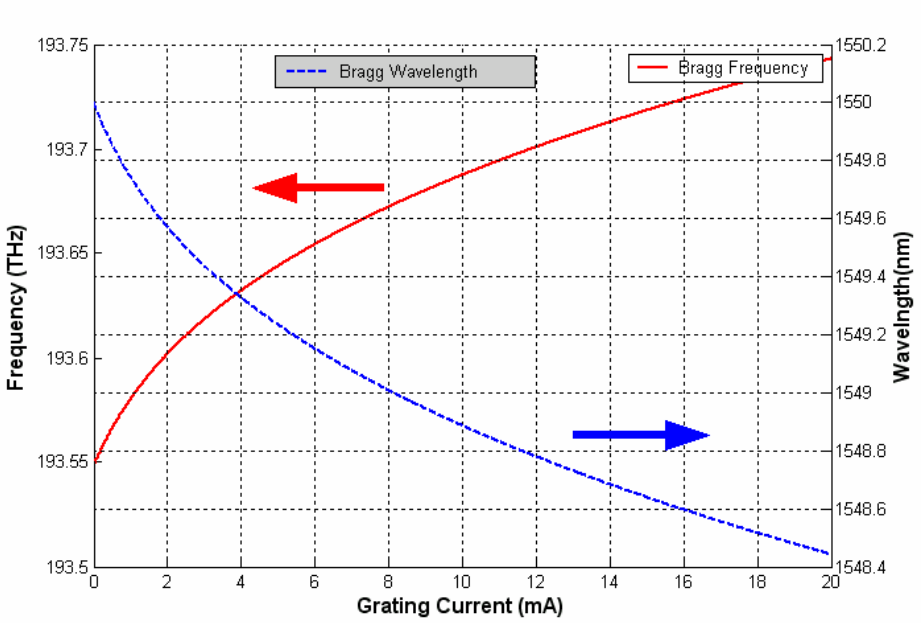

Fig. 2-12 The simulation of Bragg frequency under different grating currents

Therefore, when the current injected into the back SG section, the spectrum of the back SG reflector changes. Figure 2-13, Figure 2-14, and Figure 2-15 show the spectra of front and back SG reflectors, total reflectivity of two SG reflectors, and threshold gain under current injection into the back SG section.

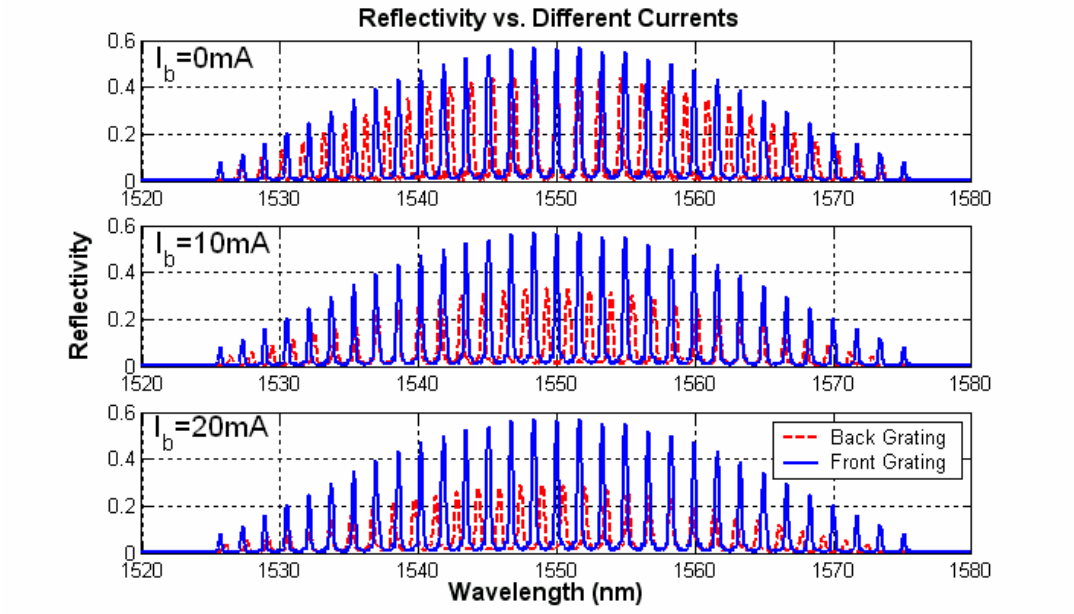

Fig. 2-13 Spectra of front and back SG reflectors under current injection into the back SG section

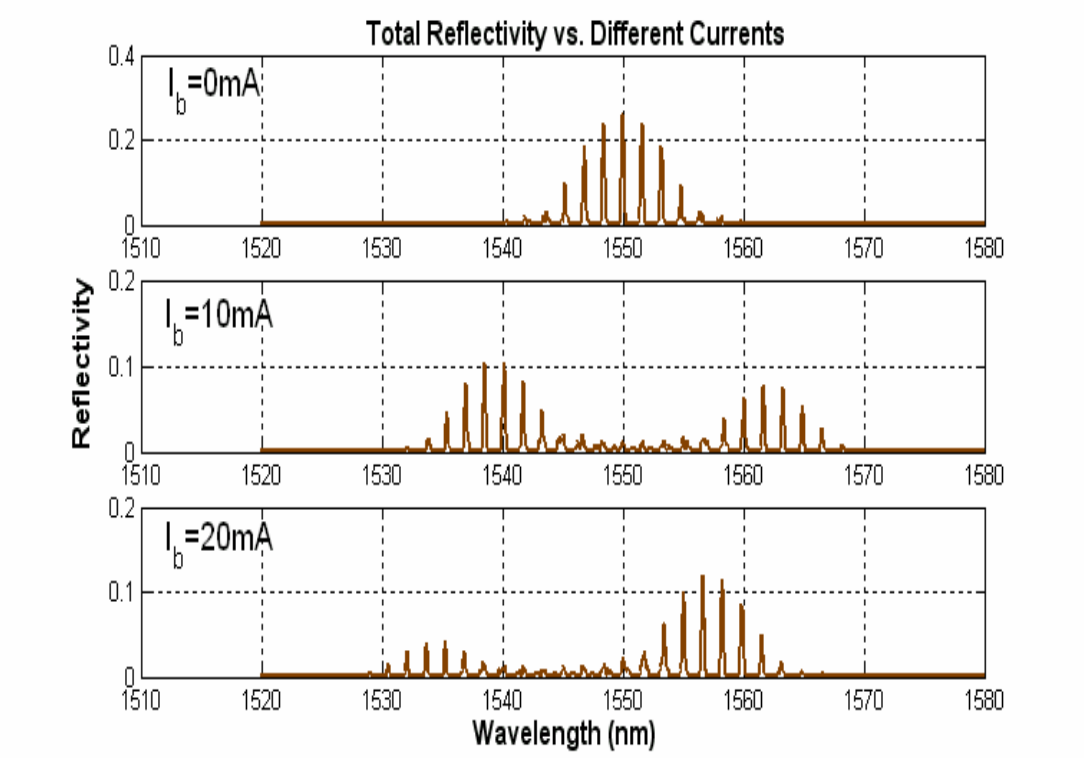

Fig. 2-14 Total reflectivity of two SG reflectors under current injection into the back SG section

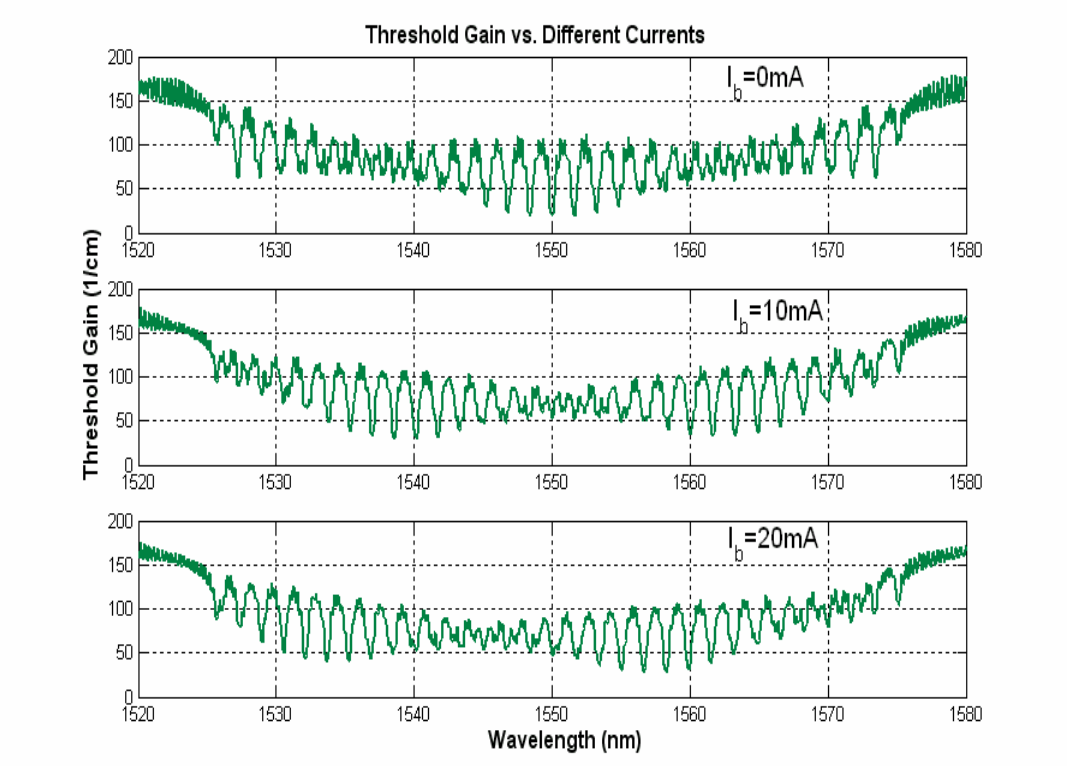

Fig. 2-15 Threshold gain under current injection into the back SG section

With the increase of the current in the back SG section, the carrier density increases and simultaneously the refractive index decreases due to the free-carrier plasma effect. For the back SG reflector this leads to an increase in the Bragg frequency. However, the absorption also increases due to free carriers and this reduces the amount of feedback to the active section. Furthermore, the spectrum for the back SG reflector shifts to shorter wavelength. The total reflectivity's maximum changes from Bragg wavelength to another. The threshold gain is the same condition as total reflectivity.

In addition, we discuss the lasing wavelength under current injection into one SG section. Basically, the coarse tunability of the SG-DBR laser is obtained by carrier injection in one SG section. This carrier injection induces a refractive index change leading to a wavelength shift of the reflector. With injection in one reflector, a coincidence between the main peak of the shifted reflector and another peak, different than the main one, of the other SG reflector is obtained, inducing the selection of another cavity mode as the lasing wavelength. With the current injection into the back SG section, the lasing wavelength shown in Fig. 2-16 changes from Bragg wavelength to shorter one as a result of the shorter peak spacing of the back SG reflector than that of the front SG reflector. On the contrary, with the current injection into the front SG section, the lasing wavelength shown in Fig. 2-17 changes from Bragg wavelength to longer one as a result of the longer peak spacing of the front SG reflector than that of the front SG reflector.

This vernier effect authorizes the enhancement of the tunability accessible in a waveguide by carrier plasma effect: a Bragg wavelength shift limited to the peak spacing difference between both SG reflectors is sufficient to produce a lasing wavelength shift equal to the peak spacing of the SG reflectivity comb.

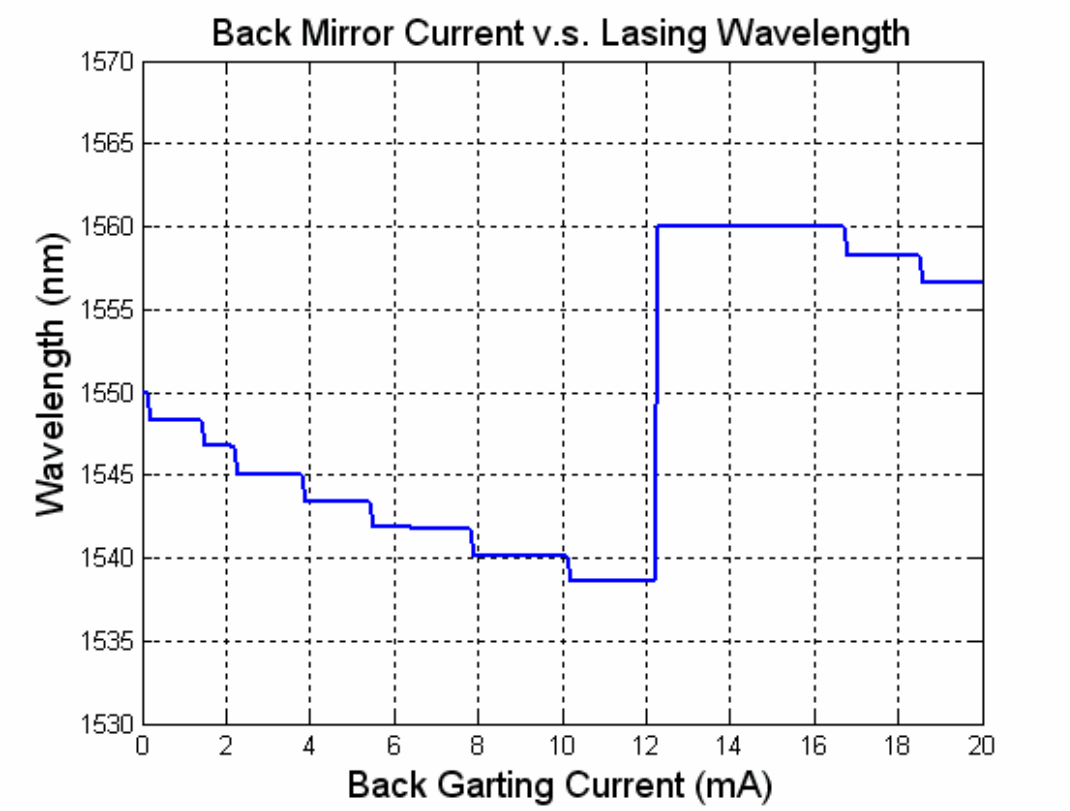

Fig. 2-16 Lasing wavelength under current injection into the back SG section

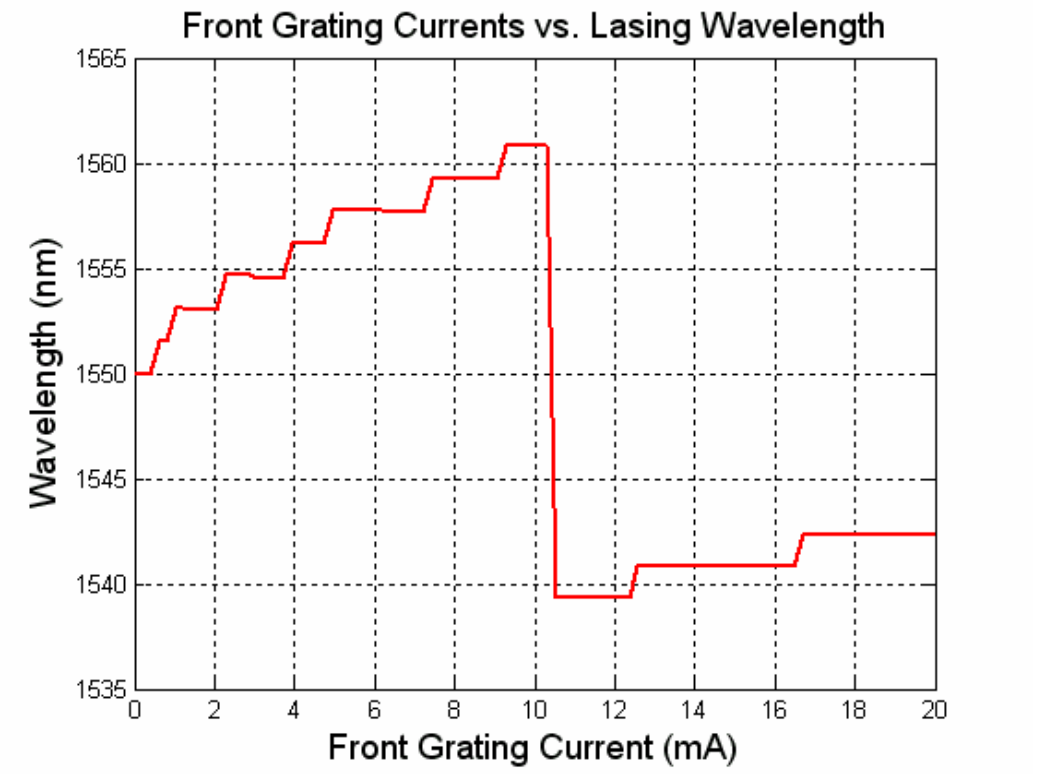

Fig. 2-17 Lasing wavelength under current injection into the front SG section

Another wavelength tunability is observed when varying both SG section currents simultaneously, to keep the coincidence between two given reflectivity peaks of the front and back reflectors. Wavelength tuning as a function of the front and back SG section currents is shown in Fig. 2-18. In this case, the equivalent reflectivity of the SG-DBR laser is shifted to select the successive cavity modes, leading to a rather fine tuning, similar to that measured on conventional DBR lasers, with a higher channel density. The same behavior is observed on all the coincidences obtained during the coarse tuning, leading to enhanced tunability for the device compared to that available on a DBR laser.

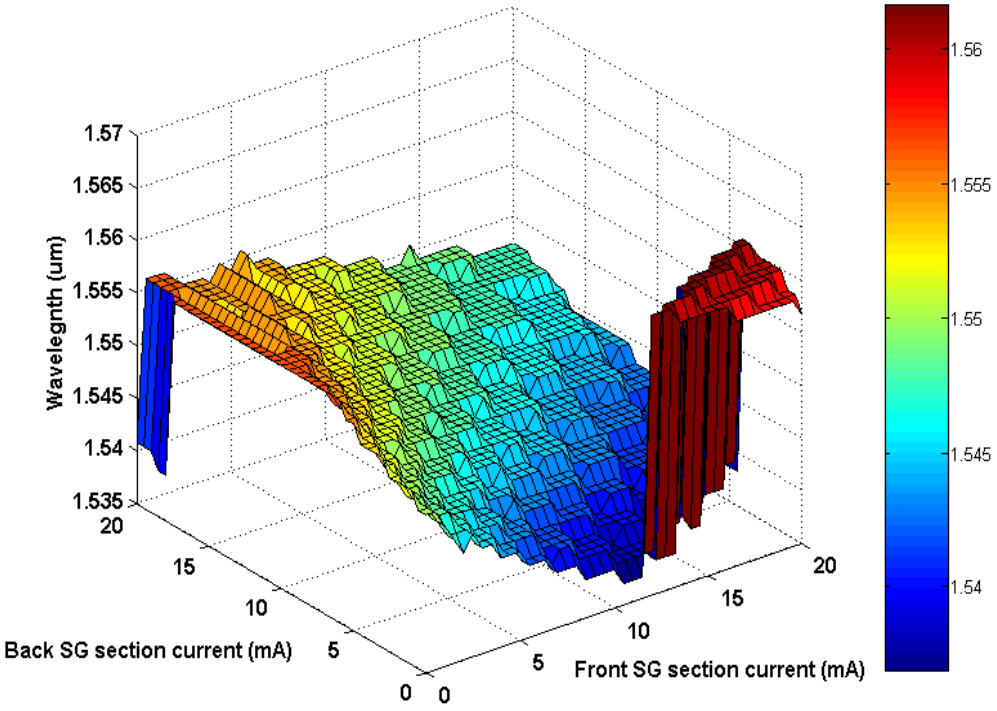

Fig. 2-18 Wavelength tuning as a function of the front and back SG section currents